Earth and Planetary Science Letters 530 (2020) 115910

Contents lists available at ScienceDirect

Earth and Planetary Science Letters

www.elsevier.com/locate/epsl

Continent-wide drainage reorganization in North America driven by mantle flow

Huilin Wang [a,b,c,*], Michael Gurnis [a], Jakob Skogseid [d]

[a] Seismological Laboratory, California Institute of Technology, Pasadena, CA, USA
[b] MOE Key Laboratory of Fundamental Physical Quantities Measurement & Hubei Key Laboratory of Gravitation and Quantum Physics, PGMF and School of Physics, Huazhong University of Science and Technology, Wuhan, China
[c] Institute of Geophysics and PGMF, Huazhong University of Science and Technology, Wuhan, China
[d] Equinor ASA, Fornebu, Norway

ARTICLE INFO

Article history:
Received 16 April 2019
Received in revised form 22 September 2019
Accepted 15 October 2019
Available online 5 November 2019
Editor: R. Bendick

Keywords:
drainage system
mantle flow
surface processes
Gulf-of-Mexico-routing drainage basin

ABSTRACT

North America (NA) experienced pronounced changes in continental-scale drainage characterized by a reversal for much of the continental interior from north into the Canadian arctic to south into the Gulf of Mexico (GoM) from the Mid-Cretaceous to the Paleocene. However, the driving mechanism for these profound drainage reorganizations remain unexplained. Here, we investigate the role of mantle flow on landscape evolution, by coupling dynamic topography with surface processes. This approach enables us to simulate catchment dynamics and the rearrangement of sediment transport in response to mantle flow. We show that a west-to-east drainage reversal can be induced by the NA overriding the subducted Farallon plate. Moreover, augmented dynamic subsidence caused by a basalt-to-eclogite transformation of an oceanic plateau within the Farallon slab, depressed the GoM region and expanded the integrated drainage to the GoM since the Early Paleocene. For the first time, we show that dynamic topography can explain the north-to-south continental-scale drainage reorganization in North America.

1. Introduction

Landscape and drainage system evolutions are the integrated results of multi-scale processes ranging from surface erosion and sedimentation, lithospheric-scale tectonics, to mantle convection. However, to what extent each process, especially the deep-seated mantle convection, shapes the ground surface remains unclear.

One region that has experienced significant landscape and drainage network changes is North America (NA). The sediment record suggests that the North American plate has undergone profound drainage reorganizations during the last ~100 Myr. Detrital zircons of the Early Cretaceous Mannville Group in the Western Canada Sedimentary Basin indicate that a north-northwest oriented drainage system was dominant in Canada and in the eastern three-quarters of NA (Fig. 1a). Concurrently, Cretaceous fluvial sandstones in the Gulf of Mexico (GoM) indicate a more restricted source region with materials mainly originating from the Mississippi Embayment, bounded by the Western Texas Plateau and Southern Appalachia (Marcher and Stearns, 1962; Galloway, 2008; Blum and Pecha, 2014).

The north-northwest sediment routing system was terminated by the Western Interior Seaway (WIS) during the Late Cretaceous (Blum and Pecha, 2014). After withdrawal of the WIS during the Late Cretaceous and Early Paleocene, the drainage system in the northern continent switched to a more northeastern orientation, where sediments derived from the Canadian Rocky Mountains were transported towards the Hudson Bay (Duk-Rodkin and Hughes, 1994) (Fig. 1b). In the southern NA, the Paleocene Wilcox Group in the GoM suggests a significantly northward expansion of the drainage basin reaching northward to the present Great Lakes and westward to the Sevier and Laramide orogenic belts (Fig. 1b; Galloway et al., 2011; Blum et al., 2017; Sharman et al., 2017). After the broad west to east drainage shift in the north and the enlargement of southward oriented fluvial network in the south, the river drainage to the GoM continued an eastward shift during the Cenozoic (Galloway et al., 2011) (Fig. 1c).

As the paleo-drainage of NA has largely been uncovered, the driving mechanism for these continental-scale reorganizations has been debated, ranging from lithospheric-scale tectonics to deeper mantle processes (Winker, 1982; Dickinson et al., 1988; Shephard et al., 2010). A pronounced tectonic event that changed lithospheric structure of NA is the Laramide orogenic uplift between ca.

* Corresponding author at: Seismological Laboratory, California Institute of Technology, Pasadena, CA, USA.
E-mail address: huilin@gps.caltech.edu (H. Wang).

https://doi.org/10.1016/j.epsl.2019.115910
0012-821X/

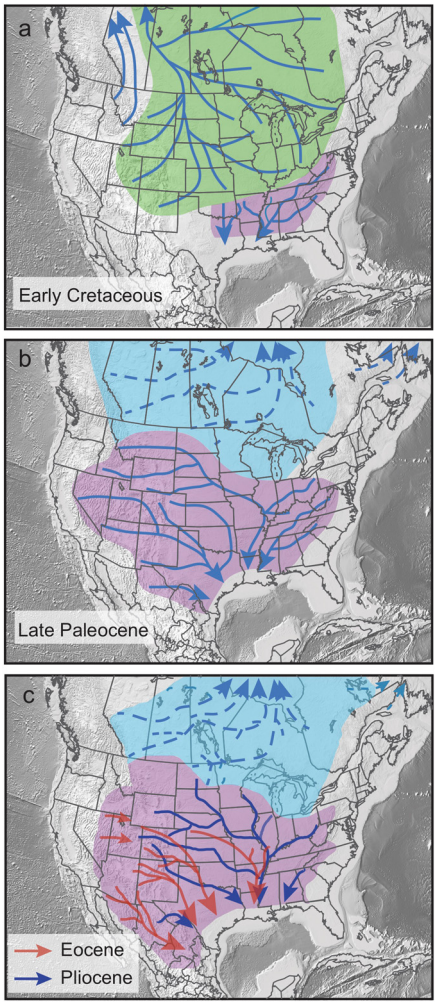

Fig. 1. Paleo-drainage evolutions in a present-day North American reference frame. **(a)** In the Early Cretaceous, north-northwest routing river system dominated in western Canada and northeastern U.S. (green shaded area), while only a small catchment area in the southernmost U.S. was drained to the GoM (Blum and Pecha, 2014) (purple shaded area). **(b)** In the Paleocene, the primary drainage in Canada changed to north-northeastward routing (Duk-Rodkin and Hughes, 1994) (blue shaded area); meanwhile, much of the U.S. drained to the GoM (Blum and Pecha, 2014). **(c)** Through the Cenozoic, the major river network in the northern continent kept routing to the north-northeast. In the south, the headwater dominated in the western and southeastern U.S. in the Eocene (red arrows), followed by a Neogene migration of the major tributaries to the central and eastern U.S. (Galloway et al., 2011) (dark blue arrows). During the Paleocene and Eocene, the dominant tributaries mostly drained the western U.S. into the northwestern GoM (Galloway, 2008). By the Neogene, multiple large rivers started to drain the eastern continent and sediments were mainly deposited in the central and eastern Gulf basin. Grey background is present-day surface topography. (For interpretation of the colors in the figure(s), the reader is referred to the web version of this article.)

80 to 55 Ma (Dickinson et al., 1988). The uplift has been linked to the increased Paleocene sediment supply derived from the Western Cordillera forming the lower Wilcox Group within the GoM, and a change of the GoM-bounding drainage area to the west (Winker, 1982).

Concurrently, dynamic topography, induced by the normal stress at the base of lithosphere originating from mantle convection, may be an additional component that can deflect the surface topography in NA (e.g., Liu and Gurnis, 2010). As NA moved westward over the subducted Farallon plate since the Early Jurassic, a broad dynamic topography signal migrated eastward (Spasojevic et al., 2009; Liu et al., 2011). Presently, the center of a dynamic low is likely located east of NA, consistent with the low residual topography (i.e. observed oceanic depth with normal thermal cooling removed) and the tomographic signature of the Farallon plate in the lower mantle (Fig. 2). However, the drainage changes in NA appear to be more complex than simply driven by the eastward migration of a dynamic topography depression, especially given the Paleocene reversal of sediment transport from northward to the Canadian Arctic sea to southward to the GoM.

Recently, seismic tomographic inversions of the deep mantle reveal a distinct lower mantle velocity/density anomaly localized below the northern GoM region, likely to be the subducted conjugate of an oceanic plateau (e.g., the Mid Pacific Mountains or Hess Rise conjugates) (Liu et al., 2010; Ko et al., 2017; Maguire et al., 2018) (Fig. 2). Formed within the Farallon plate or at the Pacific-Farallon ridge axis, the oceanic plateau with anomalously thick igneous crust probably subducted with the Farallon plate (Livaccari et al., 1981). In addition to the previously described eastward translation of a long-wavelength dynamic topography low, the basalt-to-eclogite phase transformation of the oceanic plateau is suggested to have provided an additional negative buoyancy and further caused a localized surface subsidence in the GoM region by up to 1.5 km since the Early Paleocene (Wang et al., 2017). Back-stripping of the sediment succession from seismic reflection data and boreholes in the western GoM indicate that a subsidence event, amounting to ~2 km sometime during the Late Cretaceous or Cenozoic, occurred substantially after the Jurassic rifting and sea-floor spreading in the area (Feng et al., 1994). Presently, the residual topography is about −1 km in the GoM (Hoggard et al., 2016). Coincidentally, to the north of GoM, Late Mesozoic sediments that unconformably overlay Paleozoic strata indicates that the Mississippi Embayment also experienced subsidence since the Late Cretaceous (Ervin and McGinnis, 1975). However, whether there is a direct link between the enhanced negative buoyance in the subducted Farallon plate, the rapid subsidence in GoM (Wang et al., 2017) and the broader-scale drainage system reversal in NA during the Late Cretaceous to early Paleogene remains unknown.

To unravel the role of mantle-flow-driven dynamic topography on the physiographic evolution, this study extends the dynamic topography predictions by linking them with surface processes. This approach bridges the gap between the long-wavelength dynamic topography and smaller scale processes, enabling estimation of catchment dynamics and the evolution of erosion and sedimentation. The modeling results show that the continental relief mirrors the dynamic topography and that mantle forces can control the continental-scale drainage orientation.

2. Methods

2.1. Mantle convection model and dynamic topography

We first obtain the dynamic topography through global mantle convection models in a spherical domain, using the finite element code *CitcomS* (Zhong et al., 2000), which solves the conservation of mass, momentum and energy equations with the Boussinesq approximation. Paleo-geographical constraints are incorporated into surface velocity fields and the thermal structure of lithosphere (Bower et al., 2015). This approach ensures the spatial and temporal distributions, and the buoyancy of downgoing slabs are consistent with predictions from plate reconstructions. In the reconstruction, the plates move with respect to a moving hot-spot frame of reference since 100 Ma and a paleomagnetically-derived reference frame for prior times (Seton et al., 2012). If the reconstruction of Matthews et al. (2016) is used, which has the Pacific plate fixed with respect to a Pacific hot-spot frame of reference, then we find the Mid-Pacific Mountains conjugate subducting beneath the GoM since ~65 Ma. Initial thermal structures are derived from a half-space cooling model based on the synthetic ages of ocean

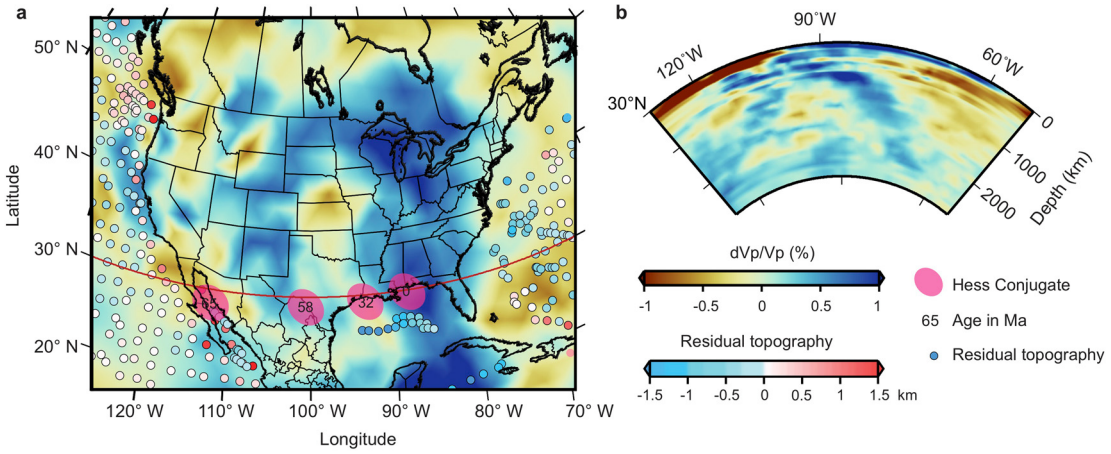

Fig. 2. Seismic observation and residual depth map. **(a)** The seismic tomography map is at 871 km depth from LLNL-G3Dv3 model (Simmons et al., 2012). The high-velocity anomaly beneath the northern GoM is interpreted to be the subducted eclogitized oceanic plateau (Liu et al., 2010; Sun et al., 2017). The colored circles are residual topography (Hoggard et al., 2016). The predicted locations of an oceanic plateau are shown by purple ellipses migrating eastward below the northern GoM (Wang et al., 2017). **(b)** Cross section of seismic tomography model LLNL-G3Dv3 at latitude of 30°N (shown as red line in Fig. 2a).

Table 1
Constant parameters for mantle convection models.

Parameter	Value
Mantle density	3300 kg/m^3
Reference viscosity (η_r)	10^{21} Pa s
Gravitational acceleration	9.8 m/s^2
Thermal expansivity	3×10^{-5} C^{-1}
Thermal diffusivity	10^{-6} m^2/s
Reference temperature	1500 °C
Surface temperature	0 °C
Earth radius	6371 km
Mantle height	2867 km
Clapeyron slope at 660 km discontinuity	−2 MPa K^{-1}

floors and simplified tectono-thermal ages of continental lithosphere (Flament et al., 2014).

The global model has $12 \times 128 \times 128 \times 64$ elements, providing lateral resolution 50×50 km at the surface and 28×28 km at the core-mantle boundary. Mesh refinement is used in the radial direction, providing ~16 km resolution at the shallow depths and lower resolution in the deep mantle. The lower boundary is free-slip and isothermal (non-dimensional temperature $T = 1$). All materials have temperature and depth-dependent viscosity

$$\eta = \eta_r \eta_0 \exp[E \times (1 - T)] \tag{1}$$

where η_r is reference viscosity (Table 1). η_0 is non-dimensional viscosity prefactor depending on depths, with value of 1 in lithosphere and upper mantle, and 30 in lower mantle. E is non-dimensional activation energy ($E = 18$ in models). T is non-dimensional temperature (normalized by temperature drop across the mantle).

The mantle-convection models cover the period from 230 Ma to the present. To obtain dynamic topography (h), we resolve the Stokes equation with a no-slip surface boundary and eliminate the buoyancy and lateral viscosity above 250 km depth, then scale radial stress (σ_{rr}) on the surface,

$$h = \frac{\sigma_{rr}}{\Delta \rho g_0} \tag{2}$$

where $\Delta\rho$ is the density difference between the upper mantle (3300 kg/m^3) and air (0 kg/m^3) for air-loaded dynamic topography. We obtained dynamic topography from two types of mantle convection models (Fig. 3). In type 1, the oceanic plateau subducted beneath the GoM has a 20 km thick crust. When it enters the eclogite stable field, the thick crust on the oceanic plateau transforms to eclogite and becomes 200 kg/m^3 denser than ambient mantle. In addition to the long-wavelength dynamic topography associated with the subducted Farallon plate, the dense oceanic plateau further depresses the GoM region by ~1.5 km since the early Paleogene (Wang et al., 2017). In type 2, the negative buoyancy of the Farallon plate only arises from its low temperatures, producing long-wavelength dynamic topography similar to previous studies (Spasojevic et al., 2009; Liu et al., 2011).

2.2. Surface process model

We then incorporate these dynamic and/or tectonic topographies to alter the changing topography which is passed through the landscape evolution model *Badlands* (Salles, 2015), in order to investigate its influence on paleo-geographic evolution. *Badlands* is a landscape evolution model that computes surface processes over hundreds to thousands of kilometers and tens of million years (Salles et al., 2017). Simplified channel and hillslope processes to track erosion and sediment transport are computed with sub-basin partitioning to balance the computational load. The continuity of mass is defined as

$$\frac{\partial z}{\partial t} = -\nabla \cdot q_s + u \tag{3}$$

where z is bedrock surface topography; u represents dynamic and/or tectonic topography change (m/yr); q_s is the depth-integrated bulk volumetric sediment flux per unit width (m^2/yr), which takes in account both channel flow (q_r) and hillslope process (q_d). The channel flow erosion uses stream power law equation

$$-\nabla \cdot q_r = -\epsilon (PA)^m (\nabla z)^n \tag{4}$$

where ϵ is an erodibility coefficient, which in our model is kept constant assuming sediment properties are temporally and spatially uniform and that there is no difference between regolith and bedrock (Table 1). P is net precipitation; m and n are constant coefficients and conventional values $m = 0.5$ and $n = 1$ are used in models; A is drainage area. Hillslope processes are defined in a linear diffusion law

$$-\nabla \cdot q_d = -k \nabla^2 z \tag{5}$$

k is the diffusion coefficient. In our models, $k = 10^{-2}$ m^2/yr in aerial and $k = 5 \times 10^{-2}$ m^2/yr in marine environment. The higher value for k in marine domain simulates the stronger smoothing effects on sediments by waves and currents.

The model domain of North American region is 8540 km × 5020 km which is gridded into an irregular triangular mesh with an averaged resolution of ~5 km. The large-scale paleo-topography at 150 Ma is constructed through removing the dynamic topography difference, Laramide uplift, sediment loading and river patterns from present-day relief model (Salles et al., 2017). We subtract the predicted dynamic topography at 0 Ma (Dyn_{0Ma}) from the global digital elevation model ETOPO1 (Amante and Eakins, 2009) (Z_{ETOPO1}), and then add the dynamic topography at 150 Ma (Dyn_{150Ma}).

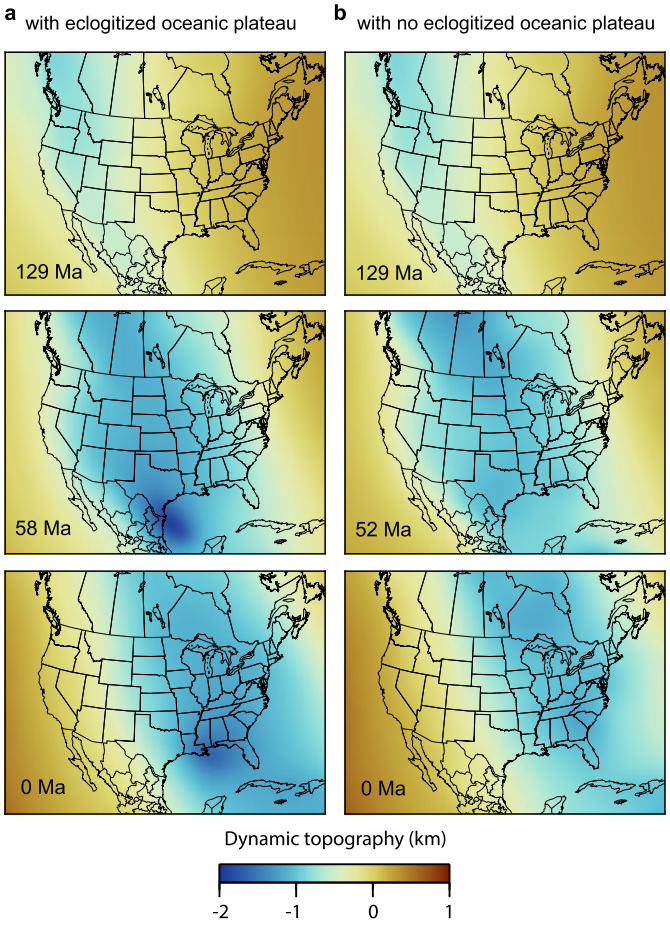

Fig. 3. Dynamic topography obtained from mantle convection models in a present-day North American reference frame. **(a)** Model 1 scenario: Dynamic topography arising both from the low-temperature Farallon plate subduction and an eclogitized oceanic plateau. **(b)** Model 2 scenario: Dynamic topography purely generated by the low-temperature Farallon plate subduction.

$$z = z_{ETOPO1} - Dyn_{0Ma} + Dyn_{150Ma} \quad (6)$$

At every 1 Myr time step, the dynamic topography variation ($Dyn_{(i-1)Ma} - Dyn_{iMa}$) is added to the model surface z to simulate changing dynamic topography. If there is no other processes working on the landscape (e.g., erosion and sedimentation), the model surface will evolve to the observed topography Z_{ETOPO1} at the present. Sediment thickness accumulated over the last 150 Myr is removed based on sediment thickness maps in the oceans (Divins, 2003) and the North American continent (Cook and Bally, 1975). The mass of removed sediments is then uniformly added to regions outside the areas of deposition in the continent. The basement depth is further adjusted by an isostatic correction (Sawyer, 1985).

The paleo-elevation of the Laramide province is not well-known (Dickinson et al., 1988) given large uncertainties in geometries and magnitudes of uplift and/or subsidence during intraplate deformation. In our starting model the elevation within the region is lowered to maximum 2 km, and the removed relief (Fig. S1) is later added back to the surface process models uniformly between 80 to 55 Ma (Dickinson et al., 1988; Fan and Carrapa, 2014). This approximation ensures a Laramide region elevation which changed its environment from deposition to erosion between 80-70 Ma.

A simple time- and spatial-dependent precipitation map is constructed based on present-day climate and plate reconstruction. The 1951-2000 precipitation model NOAA/GFDL CM2.1 (Delworth et al., 2006) is used to obtain the average precipitation rate at different latitudes. The paleo-latitudinal position of the North American plate is derived from the plate reconstruction model (Seton et al., 2012) and is used to interpolate the spatial precipitation maps at every 1 Myr since 150 Ma.

The models also have elastic plate flexure, which is solved using 2D finite difference code *gFlex* (Wickert, 2016) in *Badlands*. For NA, a bimodal elastic map is constructed. The elastic thickness is 20 km in the hot Western Cordillera and smoothly changes to 80 km in the cold craton region (Hyndman et al., 2009). Pore pressure change and sediment compaction are calculated in the sedimentary column (Bahr et al., 2001). Changes induced by sediment compaction are used to adjust both sedimentary thickness and surface elevation through time (Salles et al., 2017).

Table 2
List of surface process models.

Model	Dynamic topography	Elastic thickness (km)	Sea level	Rain (m/yr)	Erodibility (yr^{-1})	Figure
1	With Ec. oceanic plateau	Bimodal 20-80 (Hyndman et al., 2009)	Haq 87 (Haq et al., 1987)	GFDL (Delworth et al., 2006)	5×10^{-8}	4a & 6a
2	Without Ec. oceanic plateau	Bimodal 20-80 (Hyndman et al., 2009)	Haq 87 (Haq et al., 1987)	GFDL (Delworth et al., 2006)	5×10^{-8}	4b & 6b
3	None	Bimodal 20-80 (Hyndman et al., 2009)	Haq 87 (Haq et al., 1987)	GFDL (Delworth et al., 2006)	5×10^{-8}	S2
4	With Ec. oceanic plateau	40	Haq 87 (Haq et al., 1987)	GFDL (Delworth et al., 2006)	5×10^{-8}	S3a & S4a
5	With Ec. oceanic plateau	Bimodal 20-80 (Hyndman et al., 2009)	Constant	GFDL (Delworth et al., 2006)	5×10^{-8}	S3b & S4b
6	With Ec. oceanic plateau	Bimodal 20-80 (Hyndman et al., 2009)	Haq 87 (Haq et al., 1987)	1	5×10^{-8}	S3c & S4c
7	With Ec. oceanic plateau	Bimodal 20-80 (Hyndman et al., 2009)	Haq 87 (Haq et al., 1987)	GFDL (Delworth et al., 2006)	1×10^{-7}	S3d & S4d

Ec. = eclogitized.

3. Primary results from numerical modeling approach

This section presents three end-member models that have been designed to examine the influence that the subducted Farallon plate may have had on the first-order drainage evolution of NA. In Model 1 (Table 2), the dynamic topography arises from the subduction of the Farallon plate with the eclogitized oceanic plateau; in Model 2, the dynamic topography only arises from thermal variations in Farallon plate, without the oceanic plateau; and in Model 3, there is no dynamic topography associated with the Farallon subduction. Additional parameters are tested in Models 3-7 to address alternative scenarios and sensitivities.

In Model 1, the present-day dynamic topography in Model 1 predicts >1 km depression in the middle and eastern portions of NA, especially in the GoM region, caused by the subduction of the Farallon plate with the oceanic plateau (Fig. 3a). Thus, as the predicted dynamic topography at 0 Ma is removed, the reconstructed paleo-topography at 130 Ma had an elevation ~0.5 km higher in the eastern continent than in the foreland basin of the Western Cordillera (Figs. 4a and 5a). At this stage the Mississippi Embayment is predicted to have been ~0.1-0.3 km higher in elevation than the central lowlands region to the west. In response, the major modeled drainage in western Canada and northeastern U.S. routed sediments northwest to Alberta until ~68 Ma (Fig. 6a). The river outlets were localized within the foreland of the Western Cordillera. Simultaneously, river drainages to the GoM had their provenance areas limited in Texas and in the Mississippi Embayment. The low-angle subduction of the Farallon plate, in conjunction with sea-level rise (Haq et al., 1987) and flexural subsidence induced by Laramide uplift and loading, drew down the ground surface in western-central NA, which provided the accommodation space for the marine inundation between ~100-70 Ma. As the dynamic subsidence migrated eastward (Fig. 3a), the western continent rebounded at ~5 m/Myr and the marine inundation rapidly retreated by the Paleocene.

As the NA continental plate moved westward over the subducted Farallon slab, the relatively eastward translation of the dynamic subsidence simultaneously caused subsidence in the eastern continent at ~10 m/Myr. Accordingly, the plate tilting in the northern continent reversed from westward to eastward since ~63 Ma (Fig. 5a). In response to the surface slope change, the broad river polarity changed and the sediments from Canada were transported north-northeastwards toward the Hudson Bay (Fig. 6a).

Augmenting the negative buoyancy of the subducted Farallon plate, the eclogitized oceanic plateau drew down the GoM region from the Early Paleocene, thus it became the lowest region in dynamic topography (Fig. 3a). The extra subsidence induced by the oceanic plateau also caused the Mississippi Embayment to subside by ~200 m compared to the Great Lakes region (Fig. 5a). Consequently, the interior of the US tilted to the south, extending the headwater area routing to the GoM. The contrast between Model 1 and 2 demonstrates a later and more sudden southward routing in Model 1, in good agreement with the Paleocene increase in sediment flux to the GoM. Sediments derived from the Cordillera, Central Lowlands and Appalachian Mountains are here drained to the Gulf basin. Following the northward migration of GoM drainage, the major river axis and sediment transport to the GoM progressively shifted eastward with the migration of dynamic subsidence through the Cenozoic.

If there is no eclogitized oceanic plateau and the negative buoyance only arise from the low temperatures in the subducted slab, the dynamic topography generally shows a longitudinal belt of subsidence through time, but without the larger tilt to the south (Model 2; Fig. 3b). Therefore, after the removal of predicted dynamic topography at present day, the initial paleo-surface in Model 2 predicts higher relief in the eastern continent, but the

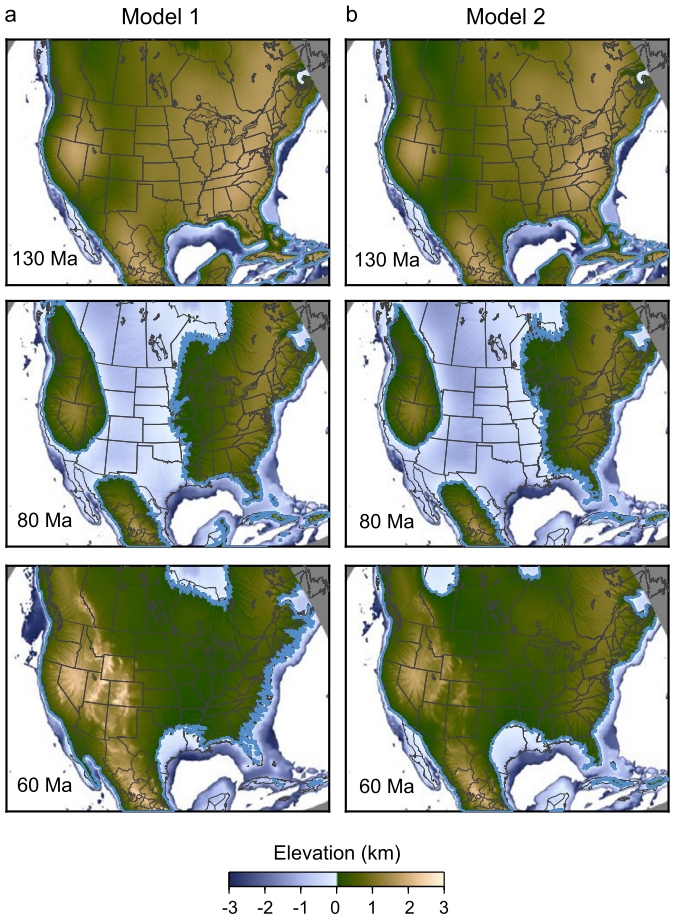

Fig. 4. Paleo-elevation maps obtained from surface process models in a present-day North American reference frame. (a) Model 1. **(b)** Model 2. The blue line represents shoreline.

Mississippi embayment remains a low relief area since 150 Ma (Figs. 4b and 5b). The drainage system in the northern continent was mainly routing north-westward, while the sediments in the eastern US were mainly flowing southward into GoM. The drainage divide already located at the southern edge of Great Lakes area in the Cretaceous. As the belt of low dynamic topography migrates eastward, Model 2 predicts marine inundation into the western-central NA continent during the Late Cretaceous. As the flooding retreated, the overall west to east sediment routing reversal in the northern continent is similar to Model 1 (Fig. 6b). On the other hand, the eastward translation of dynamic belt barely influences the north-to-south surface slope in the US region. Thus, the tributaries routed to Alberta were restricted in northernmost Cordillera and the Great Plains in the US, while the Central lowlands drained southward to the GoM since the Early Cretaceous, i.e. ~90 Myr earlier than observed.

In NA, the Laramide block uplift largely overlaps (in space and time) with the passage of dynamic topography induced by the subducted Farallon plate during last ~80 Myr. We test a model without dynamic topography modulating the continental surface (Model 3; Fig. S2; see supplementary documentation), the reconstructed paleo-surfaces since 130 Ma were similar to the present day. The sediments from Canada and western U.S. were delivered northwestward to the Hudson Bay, and a Mississippi-like fluvial system became established in the eastern US during the Early Cretaceous. The Laramide uplift advanced the steep orogenic slope from the Sevier fold and thrust belt to the eastern Wyoming and Colorado region, reshaping the detailed tributaries in the western U.S., expanding the GoM-routing drainage basin.

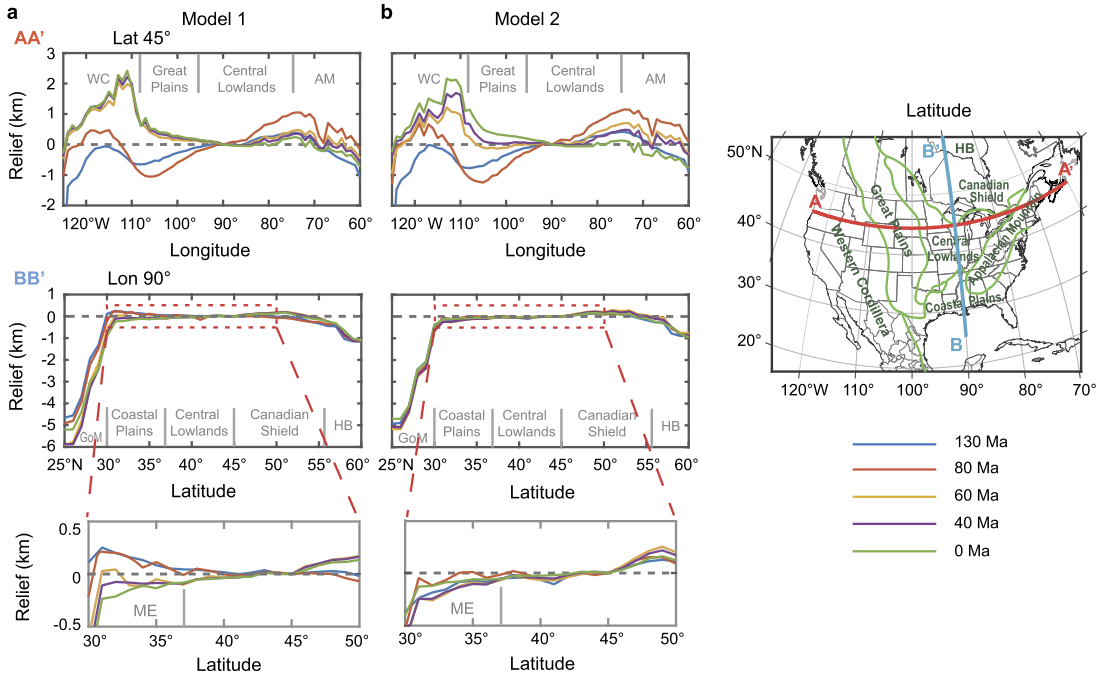

Fig. 5. Relief profiles compared to elevation at 45°N and 90°W from Model 1 **(a)** and Model 2 **(b)**. Relief profiles along latitude 45° (AA'; top panel), and along longitudinal 90° (BB'; middle and lower panels). Right panel shows physiographic provinces in North America. WC = Western Cordillera; AM = Appalachian Mountains; GoM = Gulf of Mexico; HB = Hudson Bay; ME = Mississippi Embayment.

However, the modeled Laramide uplift did not change the fundamental continental-scale drainage pattern.

The role of variations in lithosphere elasticity, sea level, precipitation and rock erodibility were explored in a series of additional models (Models 4–7; Figs. S3 and S4; see supplementary documentation). The dynamic topography and other parameters are the same as that in Model 1. These models show that within reasonable ranges, the variations of these parameters can change surface topography within a few hundreds of meters, but these factors are insufficient to change the continental tilt and the overall paleotransport directions.

4. Discussion and conclusions

NA experienced significant changes in drainage system during the Mid-Cretaceous to Paleocene (Blum and Pecha, 2014). Unlike the correlation between the migration of paleo-depositional environments and the passage of a dynamic wave described in previous studies (e.g., Spasojevic et al., 2009; Shephard et al., 2010; Eakin et al., 2014), the north-to-south migration of the main sediment drainage from the Canadian arctic to the U.S. GoM is distinct. Here, we couple the mantle derived dynamic topography with surface processes to constrain the evolution of catchment patterns and river transport directions in response to the unevenly distributed dynamic topography.

Our results demonstrate that continental-scale drainage reorganizations in NA can be an expression of deep mantle flow. As the NA plate overrode the subducted Farallon plate, the eastward translation of mantle forcing migrated the depocenter across the continent. In the far north, where the rivers previously routed westward to the Boreal sea, reversed their direction and drained to the Hudson Bay. In the U.S. region, the major river axis and the deposition center in the GoM also progressively migrated eastward in the Cenozoic, consistent with the west-to-east translation of a dynamic wave.

The uneven distribution of negative buoyancy in the Farallon plate caused by compositional variations (e.g., eclogitized oceanic plateau) further tilted the continent in a direction different from plate motion (Fig. 7). The dense oceanic plateau subducted beneath the GoM region and induced sudden Late Cretaceous subsidence in the Mississippi Embayment. In contrast to previous hypotheses (e.g., renewed extension and the passage of hotspot; Ervin and McGinnis, 1975; Cox and Van Arsdale, 2002), our results suggest the subsidence of Mississippi Embayment is related to the eclogitized oceanic plateau in the sinking Farallon plate. Consequently, the NA continent tilted to the south since the early Paleocene. Therefore, the drainage basin integrated to the GoM expanded northward to the Great Lakes region. This north-to-south river polarity reversal is distinct from the west-to-east translation of dynamic topography in NA, which is associated with the compositional variation in the subducted slab. As a result, the GoM became one of the primary depocenter in NA.

As the dynamic topography translates across the NA plate, the occurrence of Laramide uplift also largely reshaped the ground surface in the western Cordillera. We use a simplified approach to evaluate the influence of Laramide orogen event on the continental-scale drainage network, specifically the north-to-south deposition center shift from Canadian arctic to U.S. GoM. Previous studies have questioned the impact of Laramide uplift on the continental-scale reorganization of river networks. The lower Wilcox Group in GoM basin suggests an increase in sediment supply and the sediment source shift to the western U.S. in the Paleocene. But the onset of the Laramide orogeny predated the sudden sediment supply towards the GoM basin by ca. 10-15 Myr (Sharman et al., 2017). Our model (Model 3) also shows that without the dynamic forcing from the mantle, the Laramide uplift can only reshape localized drainage patterns in the western U.S., which is insufficient to switch the broad river routing direction from northwestward to southward in NA.

We note that lithospheric deformations (shortening and extension) and magmatism events are not taken into account in our models. The post-Paleocene extension and magmatism have also influenced the landscape in the Western Cordillera in NA after the Cretaceous to the Paleocene north-to-south sediment routing reversal. Lithology and climate conditions are also simplified in models. Therefore, our models provide the first-order shape and

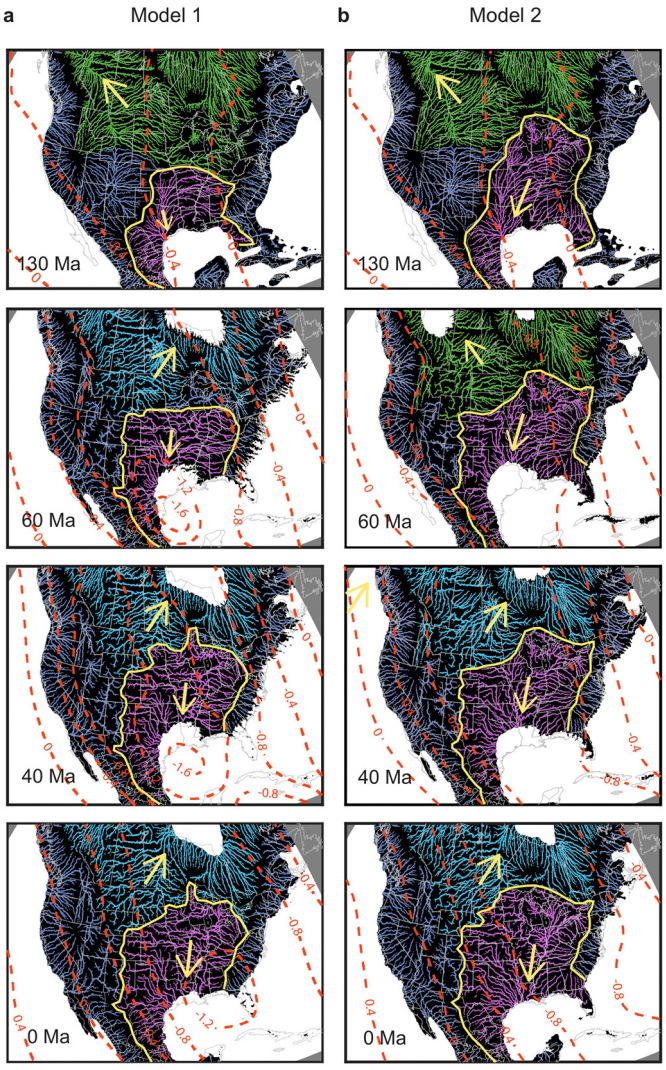

Fig. 6. Predicted paleo-drainage patterns in a North American reference frame. In Model 1 **(a)** and Model 2 **(b)**, the eastward translation of dynamic topography is driving the polarity of the fluvial system from a north-northwest (in green) to north-northeast (in blue) direction in the northern continent between the Mid-Cretaceous to Paleocene (130-60 Ma). When comparing the models for the Paleocene to Present (60-0 Ma) development, Model 1 shows a north- and eastward widening of the river networks (in purple) due to the pull-down caused by the eclogitized oceanic plateau within the Farallon plate. Yellow line outlines the GoM routing drainage basin. Arrows show broad routing directions. Dynamic topography contours are shown as red dashed lines (units in km).

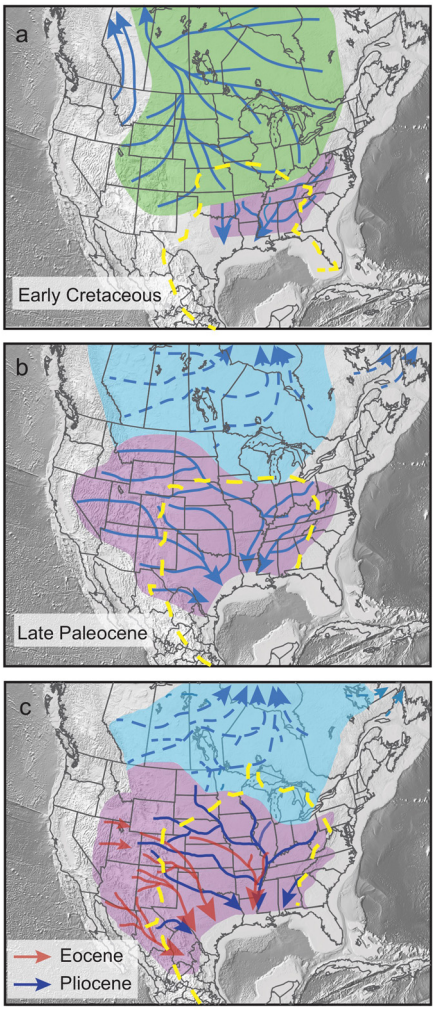

Fig. 7. Comparison of observed and modeled paleo-drainage development in NA. Dashed yellow lines show the outline of GoM drainage basin in Model 1 at 130 Ma, 60 Ma and 0 Ma, which in gross correlates with published observations according Blum and Pecha (2014), Duk-Rodkin and Hughes (1994) and Galloway et al. (2011).

characteristics of drainage evolution. Detailed changes of river network (especially in the continental margins) will need to be included in future works that have fully coupled surface processes, lithospheric deformation and mantle flow, as well as more comprehensive paleo-lithospheric and climate information.

Based on the seismic velocity/density anomaly observed in the lower mantle beneath the GoM (Ko et al., 2017; Maguire et al., 2018) and the anomalous subsidence in the Mississippi Embayment and GoM basin obtained from sediment records (Feng et al., 1994), our models demonstrate the influence of an eclogitized oceanic plateau subducted beneath the GoM region. Previous studies have proposed that a Shatsky Rise conjugate may also have subducted beneath the southern Sierra Nevada in the Late Cretaceous. The lack of a similar deep mantle velocity/density anomaly in this area may reflect that a Shatsky Rise conjugate may have remained metastable (i.e., eclogitization was either delayed or proceeded slowly), causing no major alteration of the flat slab or basement-involved Laramide deformation (Saleeby, 2003).

In Model 2, we kinematically imposed the flat slab and simplified Laramide uplift and our result, with respect to the development of WIS, is similar to previous studies (Spasojevic et al., 2009; Liu et al., 2011). The Laramide uplift is shown insufficient to change the continental-scale drainage system (Model 3). However, the fate of the Shatsky Rise conjugate remains unclear. Based on trenchward surface deflection and volcanism in the Western Cordillera, the Shatsky Rise conjugate is inferred to have been removed from the base of NA lithosphere and, according to Mix et al. (2011) and Smith et al. (2014), may have disappeared into deep mantle when the subhorizontal slab steepens in the Eocene. If, on the other hand, the slab rollback was related with eclogitization of a Shatsky Rise conjugate, this event would postdate the Cretaceous to Paleocene river reversal in NA by ~10 Myr.

In this study, we investigate the influence of mantle flow on the landscape evolution in NA. We show that the deep-seated mantle stresses could control the first-order pattern of the drainage system. The compositional variations in the subducted oceanic slab could further modulate the river networks and reverse the river routing directions. For the long-wavelength spatial and temporal scales associated with dynamic topography, the interaction between deep mantle flow and Earth's surface could be a primary control on source-to-sink pathways in sedimentary systems.

Acknowledgements

We thank two anonymous reviewers for constructive comments, and Rebecca Bendick for her editorial handling of this manuscript. H.W. and M.G. were funded by the National Science Foundation through EAR-1358646, EAR-1600956, and EAR-1645775 and by Equinor ASA. The original *CitcomS* code is obtained from Computational Infrastructure for Geodynamics (https://geodynamics.org). The *Badlands* code is obtained from https://github.com/badlands-model/badlands.

Appendix A. Supplementary material

Supplementary material related to this article can be found online at https://doi.org/10.1016/j.epsl.2019.115910.

References

Amante, C., Eakins, B.W., 2009. ETOPO1 1 arc-minute global relief model: procedures, data sources and analysis. NOAA Technical Memorandum NESDIS NGDC-24. https://doi.org/10.1594/PANGAEA.769615.

Bahr, D.B., Hutton, E.W.H., Syvitski, J.P.M., Pratson, L.F., 2001. Exponential approximations to compacted sediment porosity profiles. Comput. Geosci. 27, 691–700. https://doi.org/10.1016/S0098-3004(00)00140-0.

Blum, M., Pecha, M., 2014. Mid-cretaceous to paleocene North American drainage reorganization from detrital zircons. Geology 42, 607–610. https://doi.org/10.1130/G35513.1.

Blum, M.D., Milliken, K.T., Pecha, M.A., Snedden, J.W., Frederick, B.C., Galloway, W.E., 2017. Detrital-zircon records of Cenomanian, Paleocene, and Oligocene Gulf of Mexico drainage integration and sediment routing: implications for scales of basin-floor fans. Geosphere 13, 2169–2205. https://doi.org/10.1130/GES01410.1.

Bower, D.J., Gurnis, M., Flament, N., 2015. Assimilating lithosphere and slab history in 4-D Earth models. Phys. Earth Planet. Inter. 238, 8–22. https://doi.org/10.1016/j.pepi.2014.10.013.

Cook, T.D., Bally, A.W., 1975. Stratigraphic Atlas of North and Central America [Cartographic Material]. Princeton University Press, Princeton, NJ.

Cox, R.T., Van Arsdale, R.B., 2002. The Mississippi Embayment, North America: a first order continental structure generated by the Cretaceous superplume mantle event. J. Geodyn. 34, 163–176. https://doi.org/10.1016/S0264-3707(02)00019-4.

Delworth, T.L., Broccoli, A.J., Rosati, A., Stouffer, R.J., Balaji, V., Beesley, J.A., Cooke, W.F., Dixon, K.W., Dunne, J., Dunne, K.A., et al., 2006. GFDL's CM2 global coupled climate models. Part I: Formulation and simulation characteristics. J. Climate 19, 643–674.

Dickinson, W.R., Klute, M.A., Hayes, M.J., Janecke, S.U., Lundin, E.R., McKITTRICK, M.A., Olivares, M.D., 1988. Paleogeographic and paleotectonic setting of Laramide sedimentary basins in the central Rocky Mountain region. Geol. Soc. Am. Bull. 100, 1023–1039. https://doi.org/10.1130/0016-7606(1990)102<0256.

Divins, D.L., 2003. Total Sediment Thickness of the World's Oceans & Marginal Seas. NOAA Natl. Geophys. Data Center, Boulder, CO.

Duk-Rodkin, A., Hughes, O.L., 1994. Tertiary-quaternary drainage of the preglacial Mackenzie basin. Quat. Int. 22–23, 221–241. https://doi.org/10.1016/1040-6182(94)90015-9.

Eakin, C.M., Lithgow-Bertelloni, C., Dávila, F.M., 2014. Influence of Peruvian flat-subduction dynamics on the evolution of western Amazonia. Earth Planet. Sci. Lett. 404, 250–260. https://doi.org/10.1016/j.epsl.2014.07.027.

Ervin, C.P., McGinnis, L.D., 1975. Reelfoot rift: reactivated precursor to the Mississippi embayment. Geol. Soc. Am. Bull. 86, 1287–1295.

Fan, M., Carrapa, B., 2014. Late Cretaceous-early Eocene Laramide uplift, exhumation, and basin subsidence in Wyoming: crustal responses to flat slab subduction. Tectonics 33, 509–529. https://doi.org/10.1002/2012TC003221.

Feng, J., Buffler, R.T., Kominz, M.A., 1994. Laramide orogenic influence on late Mesozoic-Cenozoic subsidence history, western deep Gulf of Mexico basin. Geology 22, 359–362. https://doi.org/10.1130/0091-7613(1994)022<0359:LOIOLM>2.3.CO;2.

Flament, N., Gurnis, M., Williams, S., Seton, M., Skogseid, J., Heine, C., Dietmar Müller, R., 2014. Topographic asymmetry of the South Atlantic from global models of mantle flow and lithospheric stretching. Earth Planet. Sci. Lett. 387, 107–119. https://doi.org/10.1016/j.epsl.2013.11.017.

Galloway, W.E., 2008. Depositional evolution of the Gulf of Mexico sedimentary basin. In: Sedimentary Basins of the World. Elsevier. Chapter 15.

Galloway, W.E., Whiteaker, T.L., Ganey-Curry, P., 2011. History of Cenozoic North American drainage basin evolution, sediment yield, and accumulation in the Gulf of Mexico basin. Geosphere 7, 938–973. https://doi.org/10.1130/GES00647.1.

Haq, B.U., Hardenbol, J., Vail, P.R., 1987. Chronology of fluctuating sea levels since the Triassic. Science 80 (235), 1156–1167. https://doi.org/10.1126/science.235.4793.1156.

Hoggard, M.J., White, N., Al-Attar, D., 2016. Global dynamic topography observations reveal limited influence of large-scale mantle flow. Nat. Geosci. 9, 456–463. https://doi.org/10.1038/ngeo2709.

Hyndman, R.D., Currie, C.A., Mazzotti, S., Frederiksen, A., 2009. Temperature control of continental lithosphere elastic thickness, Te vs Vs. Earth Planet. Sci. Lett. 277, 539–548. https://doi.org/10.1016/j.epsl.2008.11.023.

Ko, J.Y.T., Helmberger, D.V., Wang, H., Zhan, Z., 2017. Lower mantle substructure embedded in the Farallon Plate: the Hess conjugate. Geophys. Res. Lett. 44, 10,216–10,225. https://doi.org/10.1002/2017GL075032.

Liu, L., Gurnis, M., 2010. Dynamic subsidence and uplift of the Colorado Plateau. Geology 38, 663–666. https://doi.org/10.1130/G30624.1.

Liu, L., Gurnis, M., Seton, M., Saleeby, J., Müller, R.D., Jackson, J.M., 2010. The role of oceanic plateau subduction in the Laramide orogeny. Nat. Geosci. 3, 353–357. https://doi.org/10.1038/ngeo829.

Liu, S., Nummedal, D., Liu, L., 2011. Migration of dynamic subsidence across the Late Cretaceous United States Western Interior Basin in response to Farallon plate subduction. Geology 39, 555–558. https://doi.org/10.1130/G31692.1.

Livaccari, R.F., Burke, K., Şengör, A.M.C., 1981. Was the Laramide orogeny related to subduction of an oceanic plateau? Nature. https://doi.org/10.1038/289276a0.

Maguire, R., Ritsema, J., Goes, S., 2018. Evidence of subduction related thermal and compositional heterogeneity below the United States from transition-zone receiver functions. Geophys. Res. Lett., 1–10. https://doi.org/10.1029/2018GL078378.

Marcher, M.V., Stearns, R.G., 1962. Tuscaloosa formation in Tennessee. Bull. Geol. Soc. Am. 73, 1365–1386. https://doi.org/10.1130/0016-7606(1962)73[1365:TFIT]2.0.CO;2.

Matthews, K.J., Maloney, K.T., Zahirovic, S., Williams, S.E., Seton, M., Müller, R.D., Müller, R.D., 2016. Global plate boundary evolution and kinematics since the late Paleozoic. Glob. Planet. Change 146, 226–250. https://doi.org/10.1016/j.gloplacha.2016.10.002.

Mix, H.T., Mulch, A., Kent-Corson, M.L., Chamberlain, C.P., 2011. Cenozoic migration of topography in the North American Cordillera. Geology 39, 87–90. https://doi.org/10.1130/G31450.1.

Saleeby, J., 2003. Segmentation of the Laramide Slab – evidence from the southern Sierra Nevada region. Bull. Geol. Soc. Am. 115, 655–668. https://doi.org/10.1130/0016-7606(2003)115<0655:SOTLSF>2.0.CO;2.

Salles, T., 2015. Badlands: a parallel basin and landscape dynamics model. SoftwareX 5, 195–202. https://doi.org/10.1016/j.softx.2016.08.005.

Salles, T., Flament, N., Müller, D., 2017. Influence of mantle flow on the drainage of eastern Australia since the Jurassic Period. Geochem. Geophys. Geosyst. 18, 280–305. https://doi.org/10.1002/2016GC006617.

Sawyer, D.S., 1985. Total tectonic subsidence: a parameter of distinguishing crust type at the US Atlantic continental margin. J. Geophys. Res. 90, 7751–7769. https://doi.org/10.1029/JB090iB09p07751.

Seton, M., Müller, R.D., Zahirovic, S., Gaina, C., Torsvik, T., Shephard, G., Talsma, A., Gurnis, M., Turner, M., Maus, S., Chandler, M., 2012. Global continental and ocean basin reconstructions since 200 Ma. Earth-Sci. Rev. 113, 212–270. https://doi.org/10.1016/j.earscirev.2012.03.002.

Sharman, G.R., Covault, J.A., Stockli, D.F., Wroblewski, A.F.J., Bush, M.A., 2017. Early Cenozoic drainage reorganization of the United States Western Interior-Gulf of Mexico sediment routing system. Geology 45, 187–190. https://doi.org/10.1130/G38765.1.

Shephard, G.E., Müller, R.D., Liu, L., Gurnis, M., 2010. Miocene drainage reversal of the Amazon River driven by plate-mantle interaction. Nat. Geosci. 3, 870–875. https://doi.org/10.1038/ngeo1017.

Simmons, N.A., Myers, S.C., Johannesson, G., Matzel, E., 2012. LLNL-G3Dv3: global P wave tomography model for improved regional and teleseismic travel time prediction. J. Geophys. Res., Solid Earth 117, 1–28. https://doi.org/10.1029/2012JB009525.

Smith, M.E., Carroll, A.R., Jicha, B.R., Cassel, E.J., Scott, J.J., 2014. Paleogeographic record of Eocene Farallon slab rollback beneath western North America. Geology 42, 1039–1042. https://doi.org/10.1130/G36025.1.

Spasojevic, S., Liu, L., Gurnis, M., 2009. Adjoint models of mantle convection with seismic, plate motion, and stratigraphic constraints: North America since the Late Cretaceous. Geochem. Geophys. Geosyst. 10. https://doi.org/10.1029/2008GC002345.

Sun, D., Gurnis, M., Saleeby, J., Helmberger, D., 2017. A dipping, thick segment of the Farallon Slab beneath central U.S. J. Geophys. Res., Solid Earth 122, 2911–2928. https://doi.org/10.1002/2016JB013915.

Wang, H., Gurnis, M., Skogseid, J., 2017. Rapid Cenozoic subsidence in the Gulf of Mexico resulting from Hess Rise conjugate subduction. Geophys. Res. Lett. 44, 10,930–10,938. https://doi.org/10.1002/2017GL074959.

Wickert, A.D., 2016. Open-source modular solutions for flexural isostasy: GFlex v1.0. Geosci. Model Dev. 9, 997–1017. https://doi.org/10.5194/gmd-9-997-2016.

Winker, C.D., 1982. Cenozoic shelf margins, northwestern Gulf of Mexico. Trans. Gulf Coast Assoc. Geol. Soc. 32, 427–448.

Zhong, S., Zuber, M.T., Moresi, L., Gurnis, M., 2000. Role of temperature-dependent viscosity and surface plates in spherical shell models of mantle convection. J. Geophys. Res., Solid Earth 105, 11063–11082. https://doi.org/10.1029/2000JB900003.